Chinese Journal of
POLYMER SCIENCE

RESEARCH ARTICLE

https://doi.org/10.1007/s10118-026-3800-9
Chinese J. Polym. Sci.

Nitrogen-enriched Heterocyclic Poly(ionic liquid)s/MXene Composite Membranes for Efficient Dye Separation

Jiang Li, Jun-Tao Tang, Chun Tian, Shuai Gu, Peng-Peng Shao, Rui-Ren Tang, Chen-Xiang Ai*, and Gui-Peng Yu*

Hunan Key Laboratory of Micro & Nano Materials Interface Science, Hunan Provincial Education Department; College of Chemistry and Chemical Engineering, Central South University, Changsha 410083, China

Electronic Supplementary Information

Abstract Organic dyes, as a typical class of persistent pollutants in aquatic environments, pose potential threats to ecosystem safety and public health. Poly(ionic liquid)s (PILs) can provide charge repulsion and MXene can offer interlayer nanochannels, making them ideal candidates for fabricating high-efficiency separation membranes. In this study, composite membrane materials with asymmetric and symmetric structures were facilely constructed by loading coatings of PILs-modified two-dimensional transition metal carbides (MXene, Ti_2C) at various loadings onto polypropylene microfiltration membranes, overcoming the drawbacks of poor stability of pure PIL membranes and severe interlayer stacking of neat MXene membranes, with the aim of achieving efficient separation of dye molecules. Methyl orange, methyl red, methylene blue, and rhodamine B were selected as model dyes to systematically evaluate the separation performance of the as-prepared composite membranes. The results showed that the PILs/MXene composite membranes exhibited excellent rejection performance for the four model dyes, with rejection rates exceeding 99% at higher loading levels (*e.g.*, AM-3/SM-3) while maintaining a high water flux (up to 58.36 $L{\cdot}m^{-2}{\cdot}h^{-1}{\cdot}MPa^{-1}$). The charge interaction between dyes and the membrane surface, as well as the size effect of dye molecules, were key factors that significantly affected the rejection efficiency of the membranes. In addition, the composite membrane displayed favorable operational stability in aqueous environments, demonstrating its application potential in the purification of industrial dye wastewater. This work provides new insights for the development of PILs/MXene composite membranes for dye wastewater purification, meanwhile, the simple membrane fabrication method also endows it with considerable potential for industrial scale-up.

Keywords Porous polymers; Poly(ionic liquid)s; MXene; Composite membrane; Dye separation

Citation: Li, J.; Tang, J. T.; Tian, C.; Gu, S.; Shao, P. P.; Tang, R. R.; Ai, C. X.; Yu, G. P. Nitrogen-enriched heterocyclic poly(ionic liquid)s/MXene composite membranes for efficient dye separation. *Chinese J. Polym. Sci.* https://doi.org/10.1007/s10118-026-3800-9

INTRODUCTION

Dye wastewater pollution from textile dyeing, papermaking and other chemical production processes has emerged as a serious environmental and health crisis,[1] posing persistent toxicity and significant risks to human health and aquatic life.[2] This can be addressed by removing these dyes from wastewater before they are discharged into the environment[3].

Various treatment methods, including chemical oxidation,[4] photocatalysis,[5] and electrocoagulation,[6] have been widely used to mitigate the adverse effects of dye wastewater. However, they are often pH-dependent, costly, and may produce unwanted byproducts.[7] In contrast, membrane separation technology selectively separates components without requiring phase change,[8] which also occupies minimal space, has low energy consumption, is cost-effective, and features low carbon emissions, giving it broader application potential in dye separation.[9] Lee *et al*. explored a coagulation-adsorption-microfiltration submerged membrane system to achieve efficient dye removal from dye wastewater and regenerated water production.[10]

Poly(ionic liquid)s (PILs) combine the dimensional stability and mechanical durability of polymers with the high ionic conductivity and tunable hydrophilicity and hydrophobicity properties of ionic liquids.[11] The chemical structure and properties of PIL-based membrane materials can be easily adjusted through simple anion exchange.[12] Meanwhile, the superior antibacterial activity of PILs renders them well suited for dye wastewater environments, which are prone to bacterial growth.[13] However, PILs tend to dissolve during phase separation preparation and application, leading to material loss and reduced membrane lifespan.[14] In addition, PILs typically lack stable porous structures, resulting in low permeability.

Recent advances in 2D materials, including intrinsically layered materials (*e.g.*, graphene oxide (GO)[15] and MXenes[16])

* Corresponding authors, E-mail: 22043174@csu.edu.cn (C.X.A.)
E-mail: gilbertyu@csu.edu.cn (G.P.Y.)
Special Topic: Porous Polymers
Received March 17, 2026; Accepted July 3, 2026; Published online September 10, 2026

and exfoliated nanosheets from 3D frameworks (*e.g.*, MOFs,[17] COFs[18] and zeolites[19]), have enabled the design of high-performance separation membranes. By stacking these nanosheets, well-defined interlayer nanochannels were created, providing ultrafast water transport pathways while achieving molecular sieving. Moreover, the surface chemistry of these materials (*e.g.*, charged terminations on MXenes) further enhances their selectivity *via* electrostatic interactions. Since their discovery in 2011, MXenes have been increasingly applied in environmental remediation. This is attributed to the remarkable and tunable physicochemical properties of MXenes, as well as their extremely short transport pathways and abundant nanochannels,[20] which endow them with versatile surface functionality, high adsorption efficiency, larger specific surface area and excellent hydrophobicity.[21] The unique advantages of MXenes make them ideal candidates for membrane separation materials. However, the poor flexibility prone to stacking and easy oxidation of pristine MXenes limit their practical applications.[16] To address these issues, a composite strategy can be adopted by introducing flexible materials and isolating the surface coating. Consequently, MXene-polymer composite membranes have been extensively studied. Shen *et al*. incorporated u-$Ti_3C_2T_x$ into a P84 polyimide matrix to fabricate a mixed-matrix membrane with optimized mass transport channels. The rejection rate of bromocyclohexane blue is maintained. In addition, charged MXenes can form electrostatic interactions with charged materials, making poly(ionic liquid) an ideal composite component.[22]

In this study, two methods, layer-by-layer assembly and direct mixing, were employed to fabricate composite membranes by uniformly coating PCMVImTf$_2$N and MXene (Ti_2C) onto polypropylene (PP) membranes (Fig. 1). The influence of the preparation method and loading content on dye separation performance was systematically investigated. Methyl orange, methyl red, methylene blue, and rhodamine B were selected as the model dyes to study the retention performance of the as-prepared composite membranes. The effects of the precursor and dye concentrations on the composite membrane properties were systematically investigated. The results indicated that the SM-3 membrane exhibited excellent dye retention ratio and permeability, along with good cyclic stability. Symmetrical and asymmetric membranes have provided new research ideas for dye separation.

EXPERIMENTAL

Materials and Chemicals, Synthesis of Precursor, Characterizations

The details can be found in the electronic supplementary information (ESI).

Membrane Preparation

The AM-series composite membranes were fabricated *via* a layer-by-layer vacuum filtration method. Ti_2C powder was first dispersed in anhydrous ethanol with sonication for 0.5 h, and the dispersion was filtered onto a polypropylene (PP) substrate to form a uniform layer. The PILs powder was then dispersed separately in anhydrous ethanol under sonication for 0.5 h, followed by vacuum filtration onto a Ti_2C-modified substrate to obtain the final composite membrane.

The SM-series composite membranes were prepared *via* a one-step co-deposition method. The Ti_2C and PILs powders were mixed at the same mass ratio and co-dispersed in anhydrous ethanol with sonication for 0.5 h. The homogeneous mixed dispersion was vacuum-filtered directly onto a PP substrate to form a uniform composite membrane. The Ti_2C and PILs loading of the different composite membranes are listed in Table 1.

RESULTS AND DISCUSSION

To study the impact of different film formation methods on the final dye retention performance of membrane materials, we adopted two approaches to prepare membrane materials: the first involved dispersing a certain amount of Ti_2C powder, vacuum filtering, and then dispersing a certain amount of PILs powder evenly, followed by another filtration to obtain layer-stacked membrane materials, known as asymmetric membranes (AM); the second method involved evenly dispersing Ti_2C and PILs powders, and then filtering them in one step to form mem-

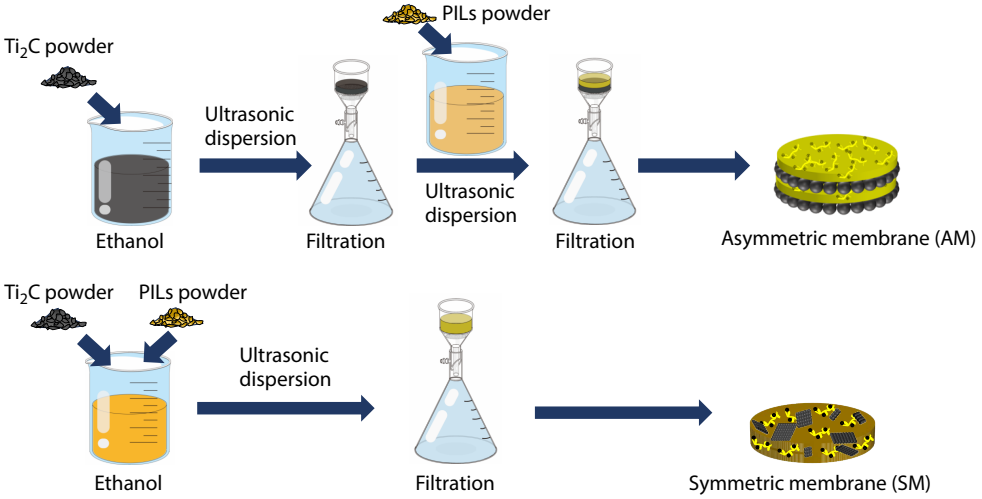

Fig. 1 The synthetic procedures for AM and SM.

https://doi.org/10.1007/s10118-026-3800-9

Table 1 Ti_2C and PILs loading amounts of different membranes.

Membrane	Ti_2C content (mg)	PILs content (mg)
AM-1	3	3
AM-2	5	5
AM-3	7	7
SM-1	3	3
SM-2	5	5
SM-3	7	7

branes, known as symmetrical membranes (SM).

The ^{1}H-NMR spectrum of PCMVImTf$_2$N is shown in Fig. 2(A). The peak at 9.8 ppm corresponds to the proton connected to the positively charged nitrogen and another nitrogen atom on the imidazolium ring. The peaks at 8 ppm were numerous and complex, corresponding to the other two protons on the imidazolium ring. The peak at 5.5 ppm corresponds to methylene protons directly connected to the cyanide group and imidazolium ring. Peaks at 3.4 and 2.6 ppm are strong and prominent, representing protons on the polymer backbone. Peak at 3.4 ppm corresponds to the protons connected to the imidazolium ring, whereas the peak at 2.6 ppm corresponds to the methylene protons on the main chain.

Fig. 2(B) shows the X-ray diffraction (XRD) pattern of the MXene precursor. The XRD pattern of Ti_2C exhibited characteristic peaks at 2θ=13.0°, 34.1°, and 60.8°, corresponding to its crystalline phase.[23] The peak observed at approximately 2θ≈40° was attributed to the partial oxidation of Ti_2C to TiO_2. From the XPS survey scanning (Fig. 2C) obtained on the sample surface in the vertical direction, we found that the sample mainly contained C, O, Ti and F. C and Ti should originate from the main structure of Ti_2C MXene, F should come from the surface group of Ti_2C MXene or the residual reactants, and O is attributed to the partial oxidation of Ti_2C to TiO_2.

The FTIR spectra of Ti_2C, PILs, and SM-3 are presented in Fig. 2(D). In the PIL spectrum, the absorption band at 2210 cm^{-1} was assigned to the cyanide group (CN) stretching vibration,[24] while the band at 1187 cm^{-1} is attributed to the symmetric stretching vibration of the imidazole ring.[25] For Ti_2C, a strong and broad band at 3427 cm^{-1} corresponds to the O—H stretching vibration,[26] indicating the presence of hydroxyl (—OH) functional groups on the carbide surface post-preparation. Additionally, the band at 1714 cm^{-1} is attributed to the characteristic C=O stretching vibration of the carboxyl (—COOH) groups.[27] Notably, all functional groups of the two substances were observed in the spectrum of SM-3. Thus, FTIR analysis not only confirmed the successful synthesis of Ti_2C and PILs but also verified the fabrication of the composite membrane.

The static contact angle, which decreases as the solid surface tension increases, serves as an indicator of the hydrophilicity or hydrophobicity of the membrane surface.[28] The static contact angles of the asymmetric and symmetric membranes are shown in Figs. 2(E) and 2(F). The water static contact angles on the surfaces of the asymmetric and symmetric membranes were 87.00° and 45.50°, respectively. The larger contact angle for the asymmetric membranes is due to the more hydrophobic PILs positioned on the surface during preparation. In contrast, in the preparation of symmetric membranes, the less dense and more hydrophilic Ti_2C powder ends up relatively on top, resulting in a smaller contact angle. This result was consistent the expected outcome.

Scanning electron microscopy (SEM) images (Fig. 3a)

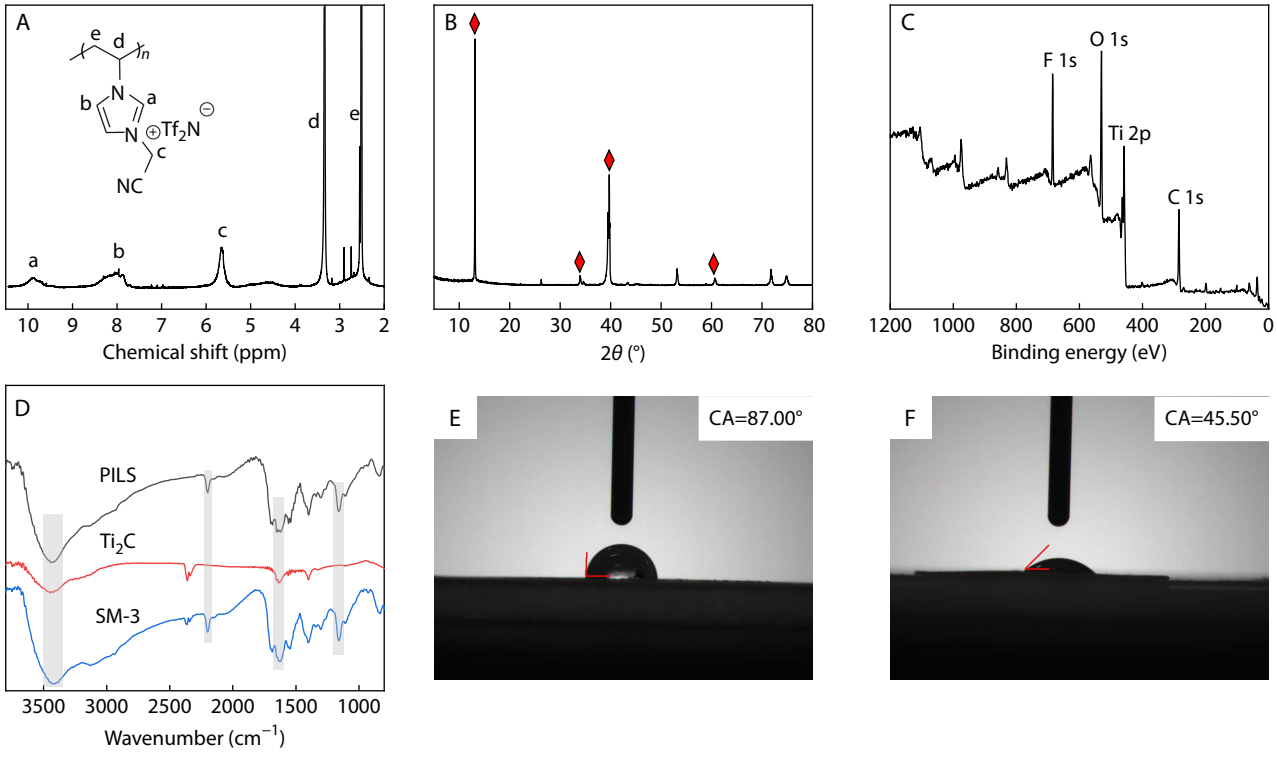

Fig. 2 (A) The ^{1}H-NMR spectrum of PCMVImTf$_2$N; (B) XRD pattern of the Ti_2C; (C) The XPS survey scanning of Ti_2C; (D) The FTIR spectra corresponding to Ti_2C, PILs and SM-3; The static contact angles of (E) the asymmetric membrane and (F) symmetric membrane.

https://doi.org/10.1007/s10118-026-3800-9

showed that the poly(ionic liquid)s consisted of numerous irregularly shaped and unevenly sized small particles, closely packed into larger particles, while the larger particles were sparsely distributed. From SEM image (Fig. 3b) of Ti_2C, typical multilayer features of Ti_2CT_x MXene were observed after treatment with HCl and LiF,[29] characterized by multiple MXene layers bound by weak van der Waals forces rather than single-layer MXene structures.[30] F^- and hydroxyl etching removes the Al layer, and the water-based etching medium provides hydrophilicity, making MXene an excellent candidate for polymer composites. The presence of numerous irregular PILs particles on the AM membrane surfaces is apparent from Fig. 3(c) because of the positioning of PILs in the upper layer during membrane material preparation. SM membrane images (Fig. 3d) show the presence of multilayer Ti_2C sheet structures, due to less dense Ti_2C occurring in the upper layer during the preparation process. The cross-sectional SEM image (Fig. 3e) shows granular PILs covering the surface with an evident lamellar structure underneath. The layered morphology is consistent with the characteristics of asymmetric membranes. In the cross-sectional SEM image (Fig. 3f) of AM, granular PILs and lamellar MXene are uniformly dispersed, presenting the typical morphology of symmetric membranes. The SEM of the membranes corroborate the contact angle measurements. To investigate the structural evolution induced by different PILs/Ti_2C loadings, the cross-sectional morphologies of the AM-1, AM-2, and AM-3 membranes were characterized using cross-sectional SEM. As shown in Figs. 3(g)–3(i), all membranes exhibit a typical asymmetric structure. The results indicated that the membrane thickness increased progressively with increasing loading. Specifically, the thicknesses of the AM-1, AM-2, and AM-3 membranes were determined to be 61.14, 67.93, and 79.16 μm, respectively. This gradual increase in thickness is consistent with the accumulation of the PILs/Ti_2C selective layer, implying an increase in the effective transport path length for water molecules.

Based on the dye separation performance experimental results shown in Figs. 4(a)–4(e) and Table 2, the areal loading of the membrane material significantly affects both the permeability and dye rejection performance; notably, increased permeability is often accompanied by reduced rejection capacity. The permeabilities of AM-1 and SM-1 membranes reached 229.30 and 382.17 $L{\cdot}m^{-2}{\cdot}h^{-1}{\cdot}MPa^{-1}$, respectively, representing relatively high levels compared to similar types of membranes reported in the literature. However, their dye rejection performance was notably poor, particularly for the SM-1 membrane, which exhibited a rejection rate of only 20.9% for methylene blue. As the areal loading gradually increased, the permeability decreased whereas the rejection rate improved substantially. Compared with other reported high-performance composite membranes for dye separation (Table 3), this work achieved a water flux of 125.86 $L{\cdot}m^{-2}{\cdot}h^{-1}{\cdot}MPa^{-1}$ while maintaining a high dye rejection rate, which is significantly higher than those in previous studies. Furthermore, a comparative analysis between AMs and SMs revealed that the SMs offer superior permeability, whereas the AMs demonstrated higher dye rejection. The enhanced permeability of

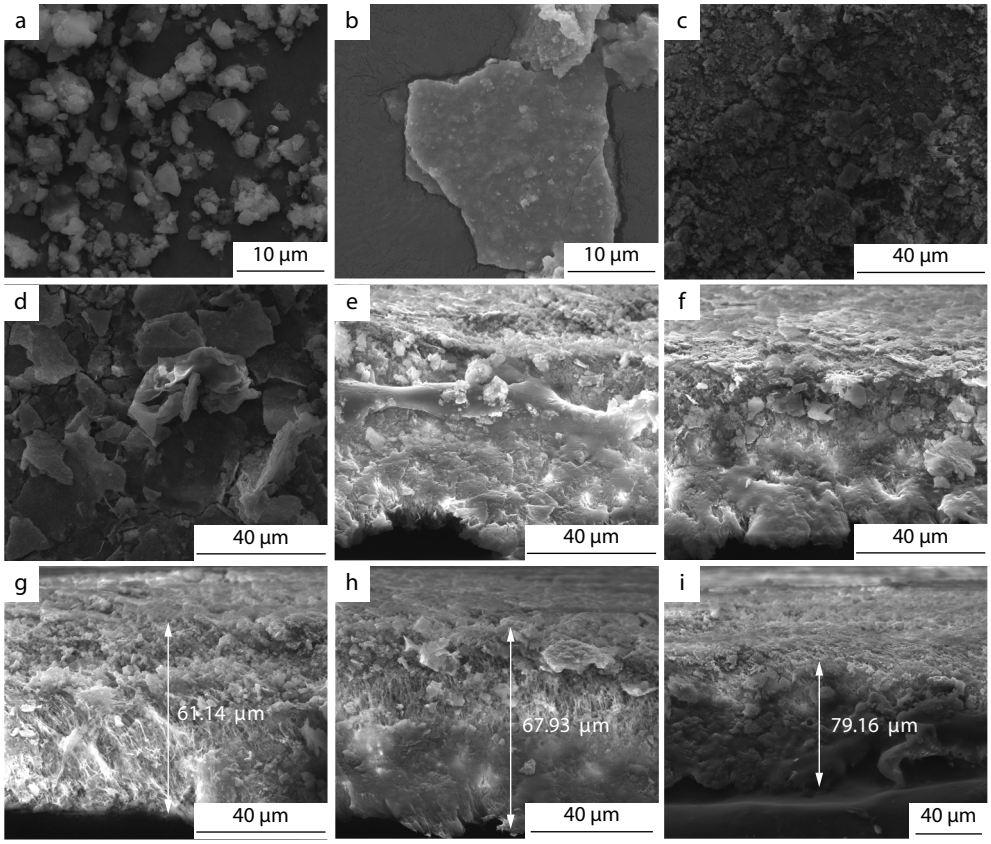

Fig. 3 Surface SEM images of (a) PILs, (b) Ti_2C, (c) AM, (d) SM and cross-sectional SEM images of (e) AM, (f) SM, (g) AM-1, (h) AM-2 and (i) AM-3.

https://doi.org/10.1007/s10118-026-3800-9

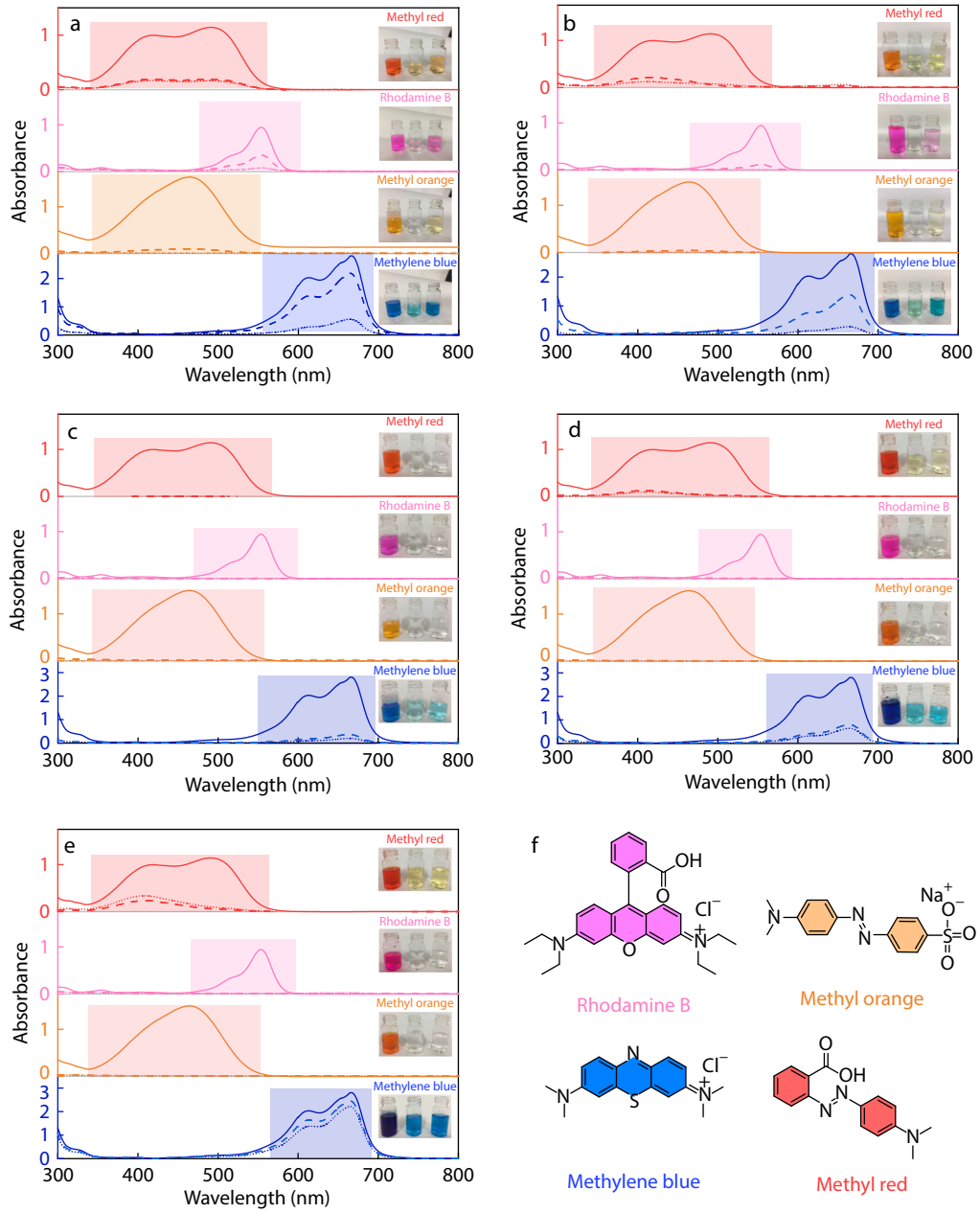

Fig. 4 UV spectra of dye retention test of membrane (a) AM-1 and SM-1, (b) AM-2 and SM-2, (c) AM-3 and SM-3 with dye concentration: 20 mg·L^{-1}, (d) AM-3 and SM-3 with dye concentration: 60 mg·L^{-1}, (e) AM-3 and SM-3 with dye concentration: 100 mg·L^{-1} (The solid line, dashed line, and dotted line represent origin solvent, SM and AM); (f) Molecular formulas of four dyes.

Table 2 Permeability and dye retention of various membranes.

Membrane	Dye concentration (mg·L^{-1})	Permeability (L·m^{-2}·h^{-1}·MPa^{-1})	Rejection ratio (%)			
			Rhodamine B	Methyl orange	Methylene blue	Methyl red
AM-1	20	229.30	92.1	99.5	80.1	83.2
SM-1	20	382.17	63.0	93.5	20.9	81.0
AM-2	20	125.86	99.5	99.8	90.0	87.5
SM-2	20	186.00	87.7	97.2	50.4	78.3
AM-3	20	47.77	>99.9	>99.9	92.8	>99.9
SM-3	20	58.36	>99.9	>99.9	87.0	99.6
AM-3	60	47.77	>99.9	>99.9	92.4	98.0
SM-3	60	58.36	>99.9	>99.9	90.5	96.1
AM-3	100	47.77	>99.9	>99.9	84.2	95.5
SM-3	100	58.36	>99.9	>99.9	82.5	93.6

https://doi.org/10.1007/s10118-026-3800-9

Table 3 The reported composite membranes for dye separation.

Membrane	Permeability ($L \cdot m^{-2} \cdot h^{-1} \cdot MPa^{-1}$)	Rejection ratio (%)	Ref.
SiO_2-PIL	189.23	Reactive black 5: 90 Reactive red 49: 85	[31]
PIL-PVDF	0.834	Acid red: 98.6 Methyl orange: 81.8 Crystal violet: 99.6 Rhodamine B: 88.3	[14]
PIL-MOF-808-PVDF	5.808	Congo red: 97.6	[32]
PIL-TiO_2-PSF	128.56	Methyl blue: 90.83 Congo red: 94.28 Evan's blue: 65.89 Methyl orange: 30.98	[33]
MXene($Ti_3C_2T_x$)-COFs	about 30	Congo red: 98.2 Chrome black T: 98.7 Methyl blue: 96.4 Methyl orange: 97.2	[18]
MXene ($Ti_3C_2T_x$)-ANF	19.53	Alcian blue: 99.1 Congo red: 96.1 Rose bengal: 98.6	[34]
Mxene-AgNW	5.13	Methyl orange: 99.2	[35]
Mxene($Ti_3C_2T_x$)-PIL	9.78	Congo red: 99.0	[36]
This work	125.86	Rhodamine B: 99.5 Methyl orange: 99.8 Methylene blue: 90.0 Methyl red: 87.5	/

SMs is attributed to the uniform mixing of PILs and Ti_2C, where Ti_2C nanosheets are randomly interspersed between the PIL particles, providing more separation channels than in composite structures. Importantly, the membrane rejection performance toward methylene blue was markedly weaker than those of the other tested dyes. Consequently, we further investigated the underlying rejection mechanisms.

The primary factors affecting dye rejection can be broadly classified into two categories: electrostatic repulsion or attraction of charged membranes and the size of the dye molecule.[37,38]

The molecular structures of the four dyes (Methyl orange, Methyl red, Methylene blue and Rhodamine B) are illustrated[39–42] in Fig. 4(f). However, the rejection of individual dye molecules through membrane pores is not solely governed by their molecular size, as dyes predominantly exist as aggregates.[43] The aggregation state is influenced by factors such as the inherent properties of the dye, concentration, pH, temperature, and electrolyte content. To elucidate the poor rejection of Methylene blue by the SM-3 membrane, two experimental approaches were designed. The electrolyte concentration was selected as the controllable variable to evaluate the effect of aggregation size as inorganic salt ions compete for solvating water to lower dye solubility and compress the electrical double layer, which weakens the electrostatic repulsion between dye molecules and induces their transition from stable dispersion to aggregation.[44–47] Three 100 mL of solutions of Methylene blue (60 mg/L) were prepared, supplemented with 1, 4, and 7 g of strong electrolyte NaCl. After filtration through the SM-3 membrane, UV-Vis spectroscopy was performed. The results showed that the membrane rejection rate for Methylene blue increased proportionally with the NaCl concentration (Fig. 5a). This experiment confirmed that the aggregate size critically governs the rejection efficiency.

To evaluate the impact of the membrane surface charge on rejection, three 10 mL aliquots of dye solutions (5 mg/L each) were prepared. Identical SM-3 membrane samples (equal in size and weight) were added, and UV-Vis measurements were taken at 1, 3 and 7 h. The results indicated that the positively

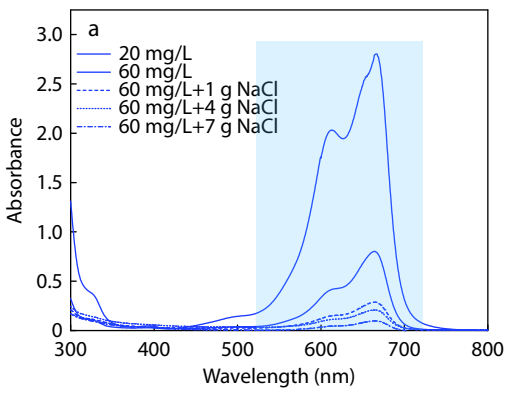

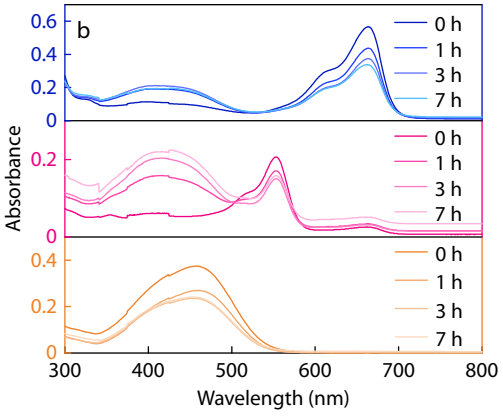

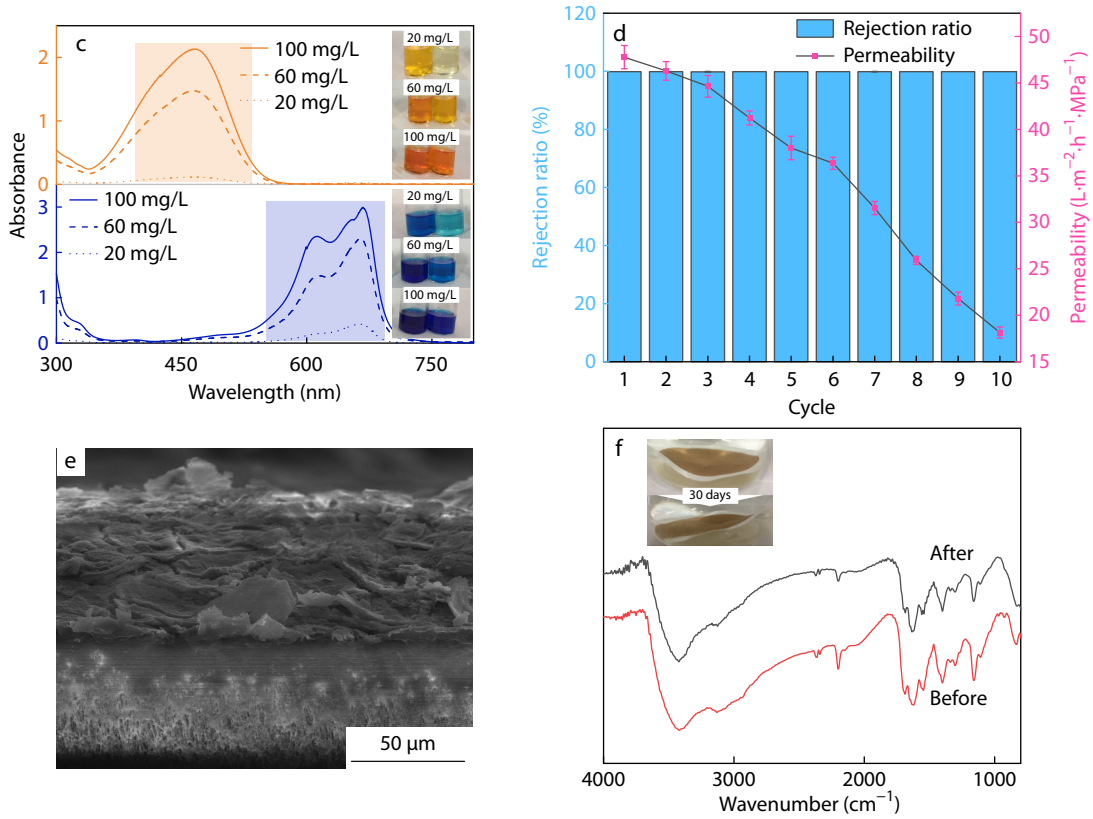

Fig. 5 (a) Effect of electrolyte concentration on methylene blue rejection performance; (b) Dye adsorption at different soaking times; (c) UV spectra of dye retention test for negatively charged SM-3 membrane; (d) Diagram of membrane cyclic performance test; (e) Cross-sectional SEM image of SM-3 after cycling; (f) The FTIR spectra of the membrane before and after soaking.

Table 4 Comparison of dye retention of positively and negatively charged SM-3 membranes.

Membrane	Dye concentration ($mg·L^{-1}$)	Permeability ($L·m^{-2}·h^{-1}·MPa^{-1}$)	Rejection ratio (%)	
			MO	MB
Positively charged	20	57.68	>99.9	87.0
	60		>99.9	90.5
	100		>99.9	92.5
Negatively charged	20	43.24	92.0	85.6
	60		66.3	73.4
	100		43.8	44.5

charged membrane exhibited slightly stronger adsorption for the anionic dye Methyl orange (MO) than for the cationic dye Methylene blue (MB) (Fig. 5b). This indicates that the surface charge from nitrogen or other heterocycles significantly influences the rejection performance. For MO, cationic adsorption may hinder permeation. To validate this, PILs and poly(acrylic acid) (PAA) powders were blended at specific ratios, dispersed in NMP solution, and stirred for 1 h. Electrostatic crosslinking occurred between positively charged PILs and negatively charged PAA chains.[48] At higher PAA content, the membrane surface was modified to a negatively charged state. Rejection tests against MO and MB solutions showed that after becoming negatively charged, the membrane exhibited smaller changes in the MB rejection rate than MO (Fig. 5c and Table 4), further confirming the critical role of electrostatic interactions in dye separation. In contrast to Methyl orange, Methyl red and Rhodamine B, Methylene blue consistently exhibited a lower rejection rate across all the membrane samples. This phenomenon cannot be solely explained by the molecular size effect, since Methyl orange possesses a smaller molecular dimension than MB, yet shows a much higher rejection. Instead, the surface charge of the membrane played a dominant role. Our membrane is positively charged under the experimental conditions shown in Fig. 5(c), which shows that the membrane has stronger adsorption toward the anionic dye Methyl orange. The electrostatic repulsion between the positively charged membrane surface and cationic MB molecules is considerably weak, which reduces the energy barrier for MB to pass through the membrane nanochannels. In contrast, the strong electrostatic attraction between the positively charged membrane and anionic methyl orange significantly enhanced its retention. This interpretation is strongly corroborated by the charge-reversal experiments in Table 4. When the membrane was converted to a negatively charged state, the rejection of anionic MO dropped sharply, while the rejection of cationic MB de-

https://doi.org/10.1007/s10118-026-3800-9

creased only moderately. Additionally, as shown in Fig. 5(a), the rejection of MB can be substantially improved by inducing dye aggregation through the addition of NaCl, indicating that the smaller aggregate size of MB under normal conditions contributes to its higher permeability. Therefore, the relatively low rejection of MB arises from the combined effect of weak electrostatic repulsion and the small effective aggregate size. In summary, the electrostatic repulsion or attraction of charged membranes and the size of the dye molecules can affect both the permeability and rejection capacity of the membrane material. However, the specific extent of their impact depends on particular conditions.

To test the recycling performance of the membranes, the SM-3 membranes were repeatedly tested for permeability and retention using 60 mg·L^{-1} of Methyl orange solutions for 10 cycles. The results are showed in Fig. 5(d). The membrane retention of Methyl orange remained above 99%, while permeability declined from 47.77 L·m^{-2}·h^{-1}·MPa^{-1} to 18.15 L·m^{-2}·h^{-1}·MPa^{-1}.

Although the flux declined, the final stabilized flux remained at a relatively high level compared with similar membrane studies treating dye-containing wastewater (Table 3). This suggests that the membrane developed in this study possesses certain advantages in terms of fouling resistance and long-term flux maintenance. Cross-sectional SEM image (Fig. 5e) of the membrane after cycling that its structure became denser than before cycling. Therefore, the observed decline in permeability is likely attributable to pore blockage caused by dye accumulation.

Similarly, to study the stability of the membranes during use, the complete membrane materials were immersed in tap water for 30 days. As shown in The FTIR spectra (Fig. 5f) of the membrane before and after soaking, the characteristic peaks of the membrane before and after soaking remained almost identical, with no significant shifts or appearance/disappearance of peaks. To further demonstrate the structural integrity of the membrane, the separation performance of the SM-3 membrane was re-evaluated after 30 days of immersion in an aqueous solution. As summarized in Table 5, the membranes exhibit excellent separation capabilities. These results confirmed that the chemical structure and selective separation channels of the SM-3 membrane were not compromised during long-term immersion, validating its robust structural stability for practical applications.

Table 5 Separation performance of SM-3 before and after soaking in aqueous solution.

Membrane	Dye concentration (mg·L^{-1})	Permeability (L·m^{-2}·h^{-1}·MPa^{-1})	Rejection ratio (%)			
			Rhodamine B	Methyl orange	Methylene blue	Methyl red
SM-3 (Before)	20	58.36	>99.9	>99.9	87.0	99.6
SM-3 (After)	20	55.72	>99.9	>99.9	88.4	99.2

CONCLUSIONS

In this study, PILs/MXene composite membranes with tunable asymmetric and symmetric structures were successfully developed on commercial PP substrate membranes. The strategic integration of PILs with MXene synergistically resolves the interlayer stacking issue of neat MXene and the instability of pure PILs, thereby effectively showing separation performance for Methyl orange, Methyl red, Methylene blue, and Rhodamine B. Benefiting from the size exclusion of MXene nanochannels and the electrostatic repulsion of PILs, the optimized membranes achieved superior dye rejection rates at higher loading levels (*e.g.*, AM-3/SM-3) while maintaining a high water flux (up to 58.36 L·m^{-2}·h^{-1}·MPa^{-1}). The facile coating strategy combined with the use of cost-effective commercial materials, offers a potential pathway for industrial scale-up. The stability of the membranes further underscores their practical viability for long-term operation in complex industrial dye wastewater treatment, providing a scalable and efficient solution for environmental remediation.

Conflict of Interests

The authors declare no interest conflict.

Electronic Supplementary Information

Electronic supplementary information (ESI) is available free of charge in the online version of this article at http://doi.org/10.1007/s10118-026-3800-9.

Data Availability Statement

The related data (DOI: 10.57760/sciencedb.j00189.00070) for this work is available in the Data Repository of China Association for Science and Technology database (https://www.scidb.cn/c/cjps), and the software for opening the data is Origin.

ACKNOWLEDGMENTS

This work was financially supported by the National Natural Science Foundation of China (Nos. 52173212, 52473224 and 22409216), Hunan Provincial Science and Technology Plan Project (No. 2024RC3287), Natural Science Foundation of Hunan Province (No. 2025JJ40010) and Natural Science Foundation of Changsha (No. kq2402208).

REFERENCES

1 Guo, X. X.; Hou, S. C.; Chen, J.; Liao, C.; He, W. D. Transpiration-prompted photocatalytic degradation of dye pollutant with AuNPs/PANI based cryogels. *Chinese J. Polym. Sci.* **2022**, *40*, 1141–1153.
2 Fayad, E.; Abu Shuheil, M.; Binjawhar, D. N.; El-Mekkawy, H. I.; Ali, H. S.; Mubarak, M. F. Activated sludge recovered from wastewater provides a sustainable approach for removing dyes and heavy metals from effluents. *Sci. Rep.* **2025**, *15*, 43225.

Graphical Abstract

Nitrogen-enriched Heterocyclic Poly(ionic liquid)s/MXene Composite Membranes for Efficient Dye Separation

Jiang Li, Jun-Tao Tang, Chun Tian, Shuai Gu, Peng-Peng Shao, Rui-Ren Tang, Chen-Xiang Ai, and Gui-Peng Yu

Central South University

In this study, PCMVImTf$_2$N/Ti$_2$C composite membranes were used to achieve efficient dye separation. The membranes at higher loading levels exhibited retention rates for four dyes: Rhodamine B, Methyl orange, Methylene blue, and Methyl red, while maintaining a high water flux.

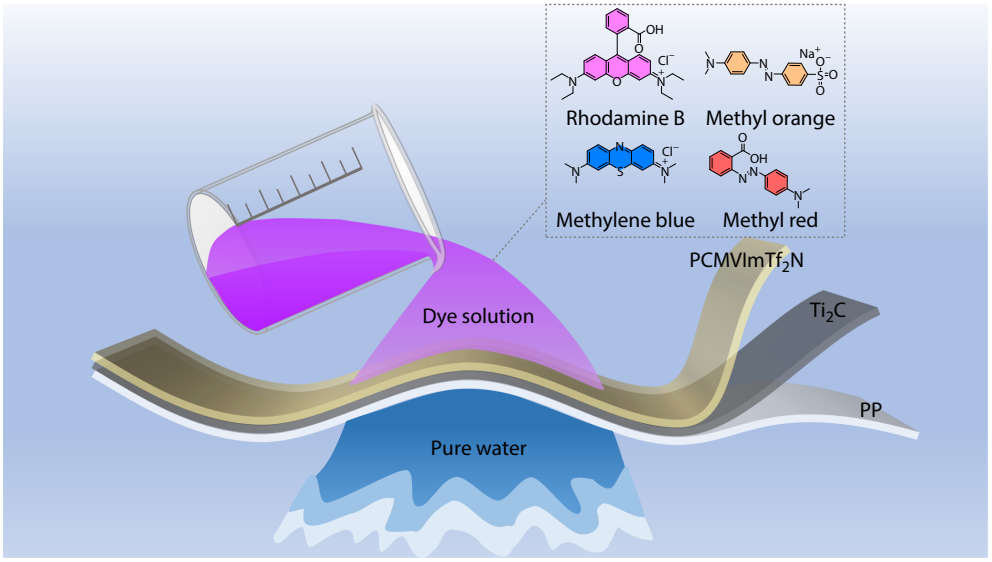

Chinese J. Polym. Sci. 2026 *https://doi.org/10.1007/s10118-026-3800-9*

3 Arola, K.; Van der Bruggen, B.; Mänttäri, M.; Kallioinen, M. Treatment options for nanofiltration and reverse osmosis concentrates from municipal wastewater treatment: a review. *Crit. Rev. Environ. Sci. Technol.* **2019**, *49*, 2049–2116.

4 Cheng, L.; Wei, M.; Huang, L.; Pan, F.; Xia, D.; Li, X.; Xu, A. Efficient H_2O_2 oxidation of organic dyes catalyzed by simple copper (II) ions in bicarbonate aqueous solution. *Ind. Eng. Chem. Res.* **2014**, *53*, 3478–3485.

5 Shishir, M. K. H.; Akand, M. S.; Maola, M.; Monira, M. F.; Rifat, M.; Sayeem, N. R.; Masud, A.; Mondal, S.; Khan, G. M. A. Photocatalytic removal of textile dyes: analytical strategies for post-degradation evaluation. *Desalination* **2026**, *617*, 119437.

6 Hakizimana, J. N.; Gourich, B.; Chafi, M.; Stiriba, Y.; Vial, C.; Drogui, P.; Naja, J. Electrocoagulation process in water treatment: a review of electrocoagulation modeling approaches. *Desalination* **2017**, *404*, 1–21.

7 Nthunya, L. N.; Chong, K. C.; Lai, S. O.; Lau, W. J.; López-Maldonado, E. A.; Camacho, L. M.; Shirazi, M. M. A.; Ali, A.; Mamba, B. B.; Osial, M.; Pietrzyk-Thel, P.; Pregowska, A.; Mahlangu, O. T. Progress in membrane distillation processes for dye wastewater treatment: a review. *Chemosphere* **2024**, *360*, 142347.

8 Zhang, S.; Shen, L.; Deng, H.; Liu, Q.; You, X.; Yuan, J.; Jiang, Z.; Zhang, S. Ultrathin membranes for separations: a new era driven by advanced nanotechnology. *Adv. Mater.* **2022**, *34*, 2108457.

9 Ding, C. T.; Yuan, J. Q.; Xie, M. Y.; Liu, Q. Y.; Yao, Z. G.; Zhang, S. Y.; Zhang, R. N.; Wu, H.; Jiang, Z. Y. Research progress in the fabrication of covalent organic framework membranes for chemical separations. *Chinese J. Polym. Sci.* **2024**, *42*, 141–158.

10 Lee, J. W.; Choi, S. P.; Thiruvenkatachari, R.; Shim, W.-G.; Moon, H. Submerged microfiltration membrane coupled with alum coagulation/powdered activated carbon adsorption for complete decolorization of reactive dyes. *Water Res.* **2006**, *40*, 435–444.

11 Qian, W.; Texter, J.; Yan, F. Frontiers in poly (ionic liquid)s: syntheses and applications. *Chem. Soc. Rev.* **2017**, *46*, 1124–1159.

12 Sun, Y.; Wu, J.; Zhu, X. Poly (ionic liquids) membranes preparation and its application. *J. Mol. Struct.* **2024**, *1304*, 137683.

13 Zheng, Z.; Xu, Q.; Guo, J.; Qin, J.; Mao, H.; Wang, B.; Yan, F. Structure–antibacterial activity relationships of imidazolium-type ionic liquid monomers, poly(ionic liquids) and poly(ionic liquid) membranes: effect of alkyl chain length and cations. *ACS Appl. Mater. Interfaces* **2016**, *8*, 12684–12692.

14 Zhang, Q.; Guo, Z.; Yuta, S. Y.; Shen, S.; Zhou, X.; Zhang, G. Blend PVDF membrane with poly(ionic liquid)-grafted silica composites showing high separation performance in dye wastewater. *J. Environ. Chem. Eng.* **2025**, *13*, 116084.

15 Tang, X.; Qu, Y.; Deng, S. L.; Tan, Y. Z.; Zhang, Q.; Liu, Q. Fullerene-regulated graphene oxide nanosheet membranes with well-

defined laminar nanochannels for precise molecule sieving. *J. Mater. Chem. A* **2018**, *6*, 22590–22598.
16 Khosla, A.; Sonu, Awan, H. T. A.; Singh, K.; Gaurav, Walvekar, R.; Zhao, Z.; Kaushik, A.; Khalid, M.; Chaudhary, V. Emergence of MXene and MXene–polymer hybrid membranes as future-environmental remediation strategies. *Adv. Sci.* **2022**, *9*, 2203527.
17 Liu, G.; Mo, B.; Guo, Y.; Chu, Z.; Ren, X. M.; Guan, K.; Miao, R.; Wang, Z.; Zhang, Y.; Ji, W.; Liu, G.; Matsuyama, H.; Jin, W. Confined-coordination induced intergrowth of metal–organic frameworks into precise molecular sieving membranes. *Angew. Chem. Int. Ed.* **2024**, *63*, e202405676.
18 Zheng, Y.; Zhang, H.; Yu, S.; Zhou, H.; Chen, W.; Yang, J. Covalently bridged MXene/COF hybrid membrane toward efficient dye separation. *Sep. Purif. Technol.* **2024**, *349*, 127908.
19 Zhou, Y.; Mu, Y.; Hsieh, M.-F.; Kabius, B.; Pacheco, C.; Bator, C.; Rioux, R. M.; Rimer, J. D. Enhanced surface activity of MWW zeolite nanosheets prepared *via* a one-step synthesis. *J. Am. Chem. Soc.* **2020**, *142*, 8211–8222.
20 Li, H.; Shi, F.; Chen, S.; Li, Y. Organic-inorganic hybrid two-dimensional membranes with enhanced solvent flux and stability. *Sep. Purif. Technol.* **2024**, *328*, 124917.
21 Ding, L.; Wei, Y.; Wang, Y.; Chen, H.; Caro, J.; Wang, H. A two-dimensional lamellar membrane: MXene nanosheet stacks. *Angew. Chem. Int. Ed.* **2017**, *56*, 1825–1829.
22 Shen, Y.; Yao, A.; Li, J.; Hua, D.; Tan, K. B.; Zhan, G.; Rao, X. Dispersive two-dimensional MXene *via* potassium fulvic acid for mixed matrix membranes with enhanced organic solvent nanofiltration performance. *J. Membr. Sci.* **2023**, *666*, 121168.
23 Wang, P.; Gao, S.; Geng, M.; Tian, J. Efficient co-catalysis of Ti2C MXene in Fenton system: promotion of Fe^{3+}/Fe^{2+} cycling. *Chem. Eng. J.* **2025**, *513*, 162832.
24 Wang, H.; Zhao, C.; Burešová, Z.; Bureš, F.; Liu, J. Cyano-capped molecules: versatile organic materials. *J. Mater. Chem. A* **2023**, *11*, 3753–3770.
25 Cai, W. A.; Cai, J. W.; Niu, H. J.; Xiao, T. D.; Bai, X. D.; Wang, C.; Zhang, Y. H.; Wang, W. Synthesis and electrochromic properties of polyimides with pendent benzimidazole and triphenylamine units. *Chinese J. Polym. Sci.* **2016**, *34*, 1091–1102.
26 Mabrouki, N.; Agougui, H.; Brahim, M.; Jabli, M.; Sonsudin, F.; Boughzala, K. Adsorption of cationic dyes from water using hydroxyapatite–pectin and hydroxyapatite–xanthan composites prepared by hydrothermal method. *Polym. Bull.* **2025**, *82*, 6691–6716.
27 Nie, H.; Du, X.; Qu, Y.; Liu, Y.; Jia, H.; Chen, Y.; Wang, Y.; Yang, W. Carboxyl-functionalized 3D imine-linked covalent organic framework for high-efficiency adsorption of cationic dyes. *Appl. Surf. Sci.* **2026**, *720*, 165373.
28 Liang, C. H.; Li, C.; Chen, T. H.; Cheng, C. Y.; Huang, C. Surface evaluation of reactive plasma-modified microporous polypropylene membrane by static contact angle analysis. *Polym. Degrad. Stabil.* **2019**, *160*, 89–95.
29 Nie, F.; Zhao, H.; Liu, S.; Li, Y.; Zhang, H.; Wu, M.; Wu, K. Laminated 2D-Ti_3C_2-MXenes as high-performance counter electrode for triiodide reduction in dye-sensitized solar cells. *Diam. Relat. Mater.* **2024**, *141*, 110586.
30 Song, H.; Ma, Y.; Yao, Q.; Liu, C.; Li, X.; Tao, X. Freeze-sonication delamination method of high crystalline-quality MXene with high yield. *Chem. Eng. J.* **2024**, *491*, 151909.
31 Yu, L.; Zhang, Y.; Wang, Y.; Zhang, H.; Liu, J. High flux, positively charged loose nanofiltration membrane by blending with poly(ionic liquid) brushes grafted silica spheres. *J. Hazard. Mater.* **2015**, *287*, 373–383.
32 Xu, L.; Liu, Y.; Wang, W.; Shen, S.; Zhang, G.; Bai, R. Highly permeable MOF-808/PVDF mixed matrix membrane assisted by ionic liquid exhibits efficient photocatalytic self-cleaning ability in the treatment of dye wastewater. *Colloids Surf. A Physicochem. Eng. Aspects* **2025**, *716*, 136722.
33 Nellur, U.; K S, K.; Naik, N. S.; Padaki, M. Innovation of poly (ionic liquid)-stabilized TiO_2 for membrane-based dye waste remediation. *J. Clean. Prod.* **2024**, *483*, 144268.
34 Li, Y.; Dai, R.; Zhou, H.; Li, X.; Wang, Z. Aramid nanofiber membranes reinforced by MXene nanosheets for recovery of dyes from textile wastewater. *ACS Appl. Nano Mater.* **2021**, *4*, 6328–6336.
35 Zhao, C.; Lu, J.; Liu, X.; Tao, R.; Li, S.; Sun, Y.; Jing, W. Electro-driven fast ion transport channels constructed in MXene/AgNWs membranes for efficient dye desalination. *Desalination* **2026**, *630*, 120175.
36 Yi, M.; Wang, M.; Wang, Y.; Wang, Y.; Chang, J.; Kheirabad, A. K.; He, H.; Yuan, J.; Zhang, M. Poly(ionic liquid)-armored MXene membrane: interlayer engineering for facilitated water transport. *Angew. Chem. Int. Ed.* **2022**, *61*, e202202515.
37 Jimenez-Solomon, M. F.; Song, Q.; Jelfs, K. E.; Munoz-Ibanez, M.; Livingston, A. G. Polymer nanofilms with enhanced microporosity by interfacial polymerization. *Nat. Mater.* **2016**, *15*, 760–767.
38 Liu, X.; Demir, N. K.; Wu, Z.; Li, K. Highly water-stable zirconium metal–organic framework UiO-66 membranes supported on alumina hollow fibers for desalination. *J. Am. Chem. Soc.* **2015**, *137*, 6999–7002.
39 Kert, M.; Skoko, J. Formation of pH-responsive cotton by the adsorption of methyl orange dye. *Polymers* **2023**, *15*, 1783.
40 Ritz, J. M.; Khakimzhan, A.; Dalluge, J. J.; Noireaux, V.; Puchner, E. M. Red light mediated photoconversion of silicon rhodamines to oxygen rhodamines for single-molecule microscopy. *J. Am. Chem. Soc.* **2025**, *147*, 7588–7596.
41 Fan, L.; Zhu, H.; Wang, K.; Liu, H.; Hu, W.; Xu, X.; Yan, S. Study on the degradation of methylene blue by Cu-doped SnSe. *Molecules* **2023**, *28*, 5988.
42 Ahmed, J.; Hassan, S.; Ahmad, M. F.; Imran, Z.; Aminullah, S.; Gulzar, A. Efficient photocatalytic degradation of methyl red dye using electrospun nanofibers: a bio-inspired approach for wastewater remediation. *J. Polym. Environ.* **2024**, *32*, 1784–1795.
43 Tantray, A.; Khan, I.; Abou-Zied, O. K.; Ali, M.; Nasser, M. S. Suppressing dye aggregation with ionic liquids: a spectroscopic study of rhodamine B in aqueous and organic media. *J. Mol. Liq.* **2025**, *437*, 128481.
44 Coates, E. Aggregation of dyes in aqueous solutions. *J. Soc. Dye. Colour.* **1969**, *85*, 355–368.
45 Koyuncu, I.; Topacik, D. Effects of operating conditions on the salt rejection of nanofiltration membranes in reactive dye/salt mixtures. *Sep. Purif. Technol.* **2003**, *33*, 283–294.
46 Cho, J.; Cho, J. K.; Lee, J.; Lee, D.; Park, C.; Kim, S. Optimization of salting-out crystallization for an efficient *in situ* separation of synthetic anthraquinone- and azo-type reactive dyes. *Sep. Purif. Technol.* **2009**, *68*, 138–144.
47 Egabaierdi, G.; Yu, H. B.; Li, Y.; Zhang, X. Q.; Song, H. O.; Du, M. X. Effect of dye aggregation and salting-out on membrane fouling and control measures during nanofiltration of saline dye wastewater. *J. Water Process Eng.* **2022**, *50*, 103285.
48 Zujovic, Z.; Chan, E. W. C.; Travas-Sejdic, J. Negatively charged poly(acrylic acid) side chains grafted onto poly(3-hexylthiophene): impact on the structural order and molecular dynamics. *Macromolecules* **2024**, *57*, 7123–7137.